Channel-encoded and SVD-assisted MIMO Multimode Transmission Schemes with Iterative Detection

Sebastian Aust, Andreas Ahrens and Steffen Lochmann
Hochschule Wismar, University of Technology, Business and Design, Philipp-Müller-Straße 14, 23966 Wismar, Germany

Keywords: Multiple-input Multiple-output (MIMO) System, Singular-value Decomposition (SVD), Bit Allocation, Optical Fibre Transmission, Multimode Fiber (MMF), Bit-interleaved Coded Modulation (BICM).

Abstract: In this contribution a coherent (2×2) MIMO (multiple input multiple output) transmission with iterative detection over a measured multimode fiber channel at 1325 nm as well as at 1570 nm operating wavelength is studied. For the channel measurements a fibre length of 1,4 km were chosen. Extrinsic information transfer (EXIT) charts are used for analyzing and optimizing the convergence behaviour of the iterative demapping and decoding. Our results show that in order to achieve the best bit-error rate, not necessarily all MIMO layers have to be activated.

1 INTRODUCTION

Energy consumption of telecom networks has been identified as an important research topic throughout the recent past since energy costs contribute significantly to network operator's operational expenditures (Baliga et al., 2009; Pickavet et al., 2008). Therefore systems enabling energy-efficient data transmission are mandatory for next generation network equipment.

In the recent past the concept of MIMO (multiple input multiple output) transmission over multimode fibers has attracted increasing interest in the optical fiber transmission community, e. g. (Bülow et al., 2010; Bülow et al., 2011; Singer et al., 2008), targeting at increased fiber capacity. The concept of MIMO transmission has been investigated since decades now for both, twisted-pair copper cable transmission – suffering from crosstalk between neighbouring wire pairs – (Van Etten, 1975; Ahrens and Lange, 2006), as well as for multi-antenna radio systems – where signal interference occurs on the radio interface (Telatar, 1999; Foschini, 1996).

A MIMO approach where modal dispersion is exploited, rather than avoided, is a promising solution. Note that for a long time the multipath nature of wireless channels was viewed as a limiting factor to be avoided. In recent years it has been realized that the multipath nature of a channel can actually enhance throughput and improve the quality of the data transmission (i. e. minimize the bit-error rate) if it is properly exploited (Ahrens and Benavente-Peces, 2009b).

Bit-interleaved coded modulation (BICM) was designed for bandwidth efficient transmission over fading channels (Caire et al., 1998; Chindapol, 2001). Wireless MIMO-BICM transmission schemes for both non-frequency and frequency selective MIMO channels have attracted a lot of attention and reached a state of maturity (Kühn, 2006; Ahrens and Benavente-Peces, 2009a). By contrast, MIMO-aided optical systems require substantial further research (Shah et al., 2005; Hsu et al., 2006; Lenz et al., 2004). That is why in addition to bit loading algorithms in this contribution the benefits of channel coding are also investigated. The proposed iterative decoder structures employ symbol-by-symbol soft-output decoding based on the Bahl-Cocke-Jelinek-Raviv (BCJR) algorithm and are analyzed under the constraint of a fixed data throughput (Bahl et al., 1974).

Against this background, the novel contribution of this paper is that we jointly optimize the number of activated MIMO layers and the number of bits per symbol combined with powerful error correcting codes under the constraint of a given fixed data throughput and integrity. The performance improvements are exemplarily studied by computer simulations at a measured 1,4 km multimode MIMO fiber channel at 1325 nm and at 1570 nm operating wavelength.

Since the "design-space" is large, a two-stage optimization technique is considered. Firstly, the un-

Aust S., Ahrens A. and Lochmann S..
Channel-encoded and SVD-assisted MIMO Multimode Transmission Schemes with Iterative Detection.
DOI: 10.5220/0004018203530360
In *Proceedings of the International Conference on Data Communication Networking, e-Business and Optical Communication Systems* (OPTICS-2012), pages 353-360
ISBN: 978-989-8565-23-5

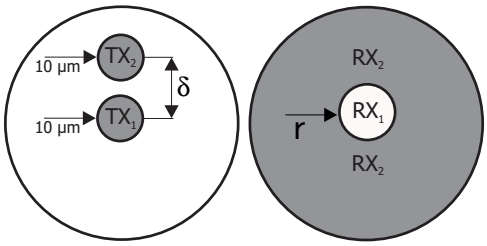

Figure 1: Forming the optical MIMO channel (left: light launch positions at the transmitter side with a given eccentricity δ, right: spatial configuration at the receiver side as a function of the mask radius r).

coded MIMO scheme is analyzed, investigating the allocation of both the number of bits per modulated symbol and the number of activated MIMO layers at a fixed data rate. Secondly, the optimized uncoded system is extended by incorporating bit-interleaved coded modulation using iterative detection (BICM-ID), whereby both the uncoded as well as the coded systems are required to support the same user data rate within the same bandwidth.

The remaining part of this contribution is organized as follows: Section 2 introduces our system model, while the proposed uncoded solutions are discussed in section 3. In section 4 the channel encoded MIMO system is introduced. The associated performance results are presented and interpreted in section 5. Finally, section 6 provides our concluding remarks.

2 CHANNEL MEASUREMENTS AND MIMO SYSTEM MODEL

Forming the MIMO (multiple input multiple output) system, the corresponding optical transmitter as well as receiver side configuration is depicted in Fig. 1. At the receiver side different spatial filters have been produced by depositing a metal layer at fiber end-faces and subsequent ion milling (Pankow et al., 2011). Details on the transmission model, which has been determined by channel measurements, are given in (Pankow et al., 2011).

2.1 MIMO Channel Measurements

For the investigated optical MIMO channel an eccentricity δ of 10 μm and a mask radius r of 15 μm were chosen (Fig. 1). The arising electrical (2×2) MIMO channel is highlighted in Fig. 2.

The obtained MIMO channel impulse responses at 1325 nm and 1570 nm operating wavelength are depicted in Fig. 3 and Fig. 4, respectively and show the expected dependency from the operating wavelength. The measured MIMO channel impulse responses at 1325 nm operating wavelength are highlighted in Fig. 3 and illustrate the activation of different mode groups according to the transmitter side light launch conditions (Fig. 1). The individual mode groups are clearly separated since almost no chromatic dispersion is imminent at the wavelength of 1325 nm. At a higher operating wavelength, i. e. 1570 nm, the separation of the different mode groups disappears based on the additional effect of the chromatic dispersion (Fig. 4).

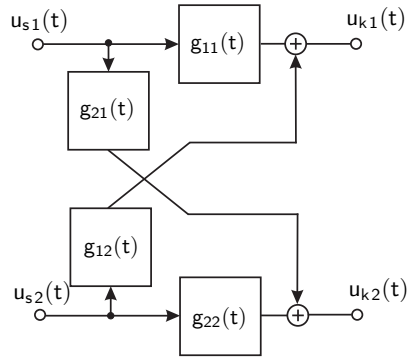

Figure 2: Electrical (2×2) MIMO system model.

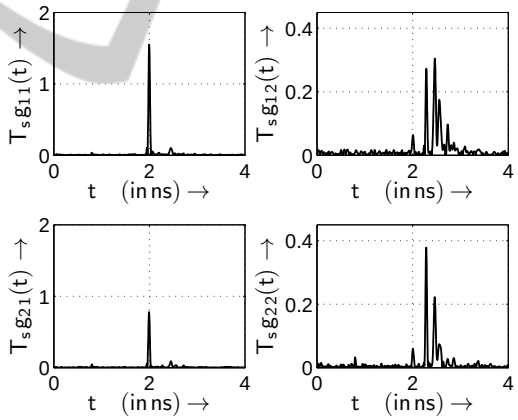

Figure 3: Measured electrical MIMO impulse responses with respect to the pulse frequency $f_T = 1/T_s = 5,12$ GHz at 1325 nm operating wavelength.

2.2 MIMO Channel Parameters

In MMF two different sources of dispersion take place, i. e. modal and chromatic dispersion. The modal dispersion can be approximated by a weighted Dirac delta impulse response

$$g_m^{(\nu\mu)}(t) = \sum_{\kappa=0}^{N-1} g_{m\kappa}^{(\nu\mu)} \, \delta(t - \tau_0 - \tau_\kappa) \ . \qquad (1)$$

Therein, N is the number of propagating modes (i. e. mode groups), $g_{m\kappa}^{(\nu\mu)}$ describes the attenuation of the

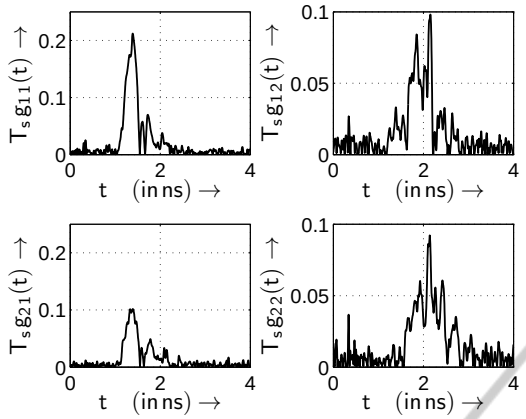

Figure 4: Measured electrical MIMO impulse responses with respect to the pulse frequency $f_T = 1/T_s = 5,12$ GHz at 1570 nm operating wavelength.

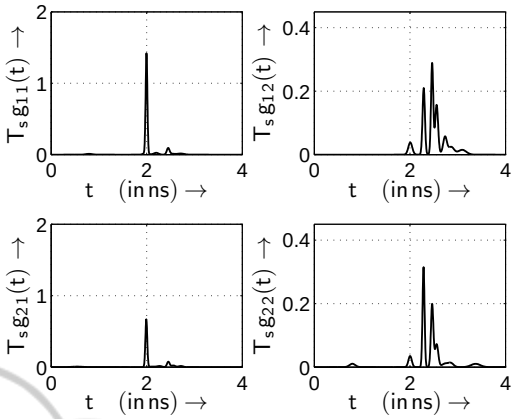

Figure 5: Approximated electrical MIMO impulse responses with respect to the pulse frequency $f_T = 1/T_s = 5,12$ GHz at 1325 nm operating wavelength by using Matlabs® curve fitting tool.

κth propagation mode (i. e. mode group) between the μth input and the νth output, τ_κ is the differential modal delay with respect to the overall baseline delay of τ_0. In the presence of modal coupling, the attenuation factor $g_{m\kappa}^{(\nu\mu)}$ would become time-varying. Taking the different SISO (single input single output) channels into consideration, the value $g_{m\kappa}^{(\nu\mu)}$ expresses the different contributions of the individual mode groups to the SISO channels within the MIMO system. Since almost no chromatic dispersion is imminent at the wavelength of 1325 nm, the individual mode groups are clearly separated as highlighted in Fig. 3.

As a result of the modal dispersion at the receiver side, a single transmitted pulse may spread into a number of adjacent symbol periods, depending on the data rate, distance traveled, and fiber properties (Singer et al., 2008). Practically, the weighted Dirac delta pulses can be approximated by Gaussian pulses. Fig. 5 shows the obtained impulse responses by using Matlabs® curve fitting tool.

Another limit for MMF is given by the chromatic dispersion, based on the frequency-dependence of the phase velocity of a wave. The transfer function of the chromatic dispersion is given by

$$G_c(f) = e^{(\pi f \tau_c)^2} \quad . \tag{2}$$

Therein, the spectral width affecting parameter τ_c results in

$$\tau_c = D_c \cdot \delta_\lambda \cdot \ell \quad , \tag{3}$$

with the parameter ℓ describing the fibre length. The parameter δ_λ represents the spectral width of the source and D_c is the group delay dispersion parameter, which depend on the refractive index *n* and the operating wavelength λ, and is described as

$$D_c = -\frac{\lambda}{c} \cdot \frac{d^2 n}{d\lambda^2} \quad . \tag{4}$$

In this work a fibre length of $\ell = 1{,}4$ km is chosen. The spectral width of the source is $\delta_\lambda = 11$ nm and the group delay dispersion parameter is assumed to be $D_c = 18$ ps/(nm·km). The impulse response of the chromatic dispersion $g_c(t)$ can be obtained by the inverse Fourier transform of (2).

Finally, the multi-mode channel impulse response between the μth input and the νth output can be obtained as

$$g_{\nu\mu}(t) = g_m^{(\nu\mu)}(t) * g_c(t) \quad . \tag{5}$$

Fig. 6 shows the obtained SISO impulse responses with modal and chromatic dispersion within the MIMO system by using Matlabs® curve fitting tool.

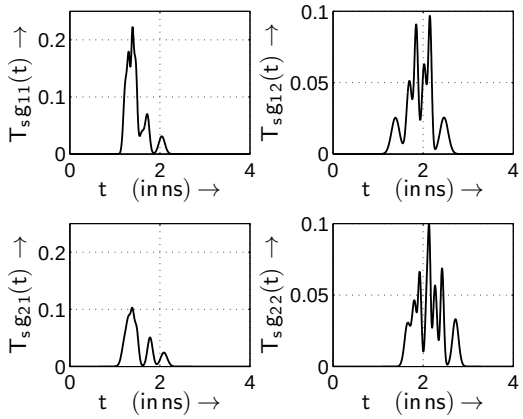

Figure 6: Approximated electrical MIMO impulse responses with respect to the pulse frequency $f_T = 1/T_s = 5,12$ GHz at 1570 nm operating wavelength by using Matlabs® curve fitting tool.

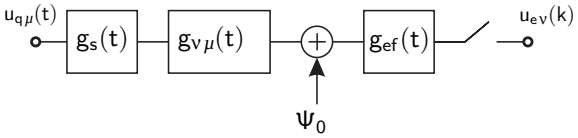

Figure 7: Mathematical representation of the MIMO related single input single output (SISO) channels.

2.3 MIMO System Model

Fig. 7 illustrates the MIMO related single input single output (SISO) channels. Rectangular pulses are used for transmit and receive filtering. The baseband finite-length impulse response of the MIMO channel between the μth input and the νth output is given by

$$h_{\nu\mu}(t) = g_s(t) * g_{\nu\mu}(t) * g_{ef}(t) \quad . \tag{6}$$

The impulse responses of the transmit and receive filtering are described by $g_s(t)$ and $g_{ef}(t)$.

The block diagram of the transmission model is shown in Fig. 8: Coherent transmission and detection is assumed together with the modulation format QAM (quadrature amplitude modulation) per MIMO transmission mode. The block-oriented system for frequency selective channels is modelled by:

$$\mathbf{u} = \mathbf{H} \cdot \mathbf{c} + \mathbf{w} \quad . \tag{7}$$

In (7), the transmitted signal vector **c** is mapped by the channel matrix **H** onto the received vector **u**. Finally, the vector of the additive, white Gaussian noise (AWGN) is defined by **w** (Pankow et al., 2011; Raleigh and Cioffi, 1998). Details on the transmission model are given in (Pankow et al., 2011).

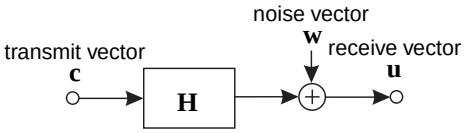

Figure 8: Transmission system model.

In MIMO communication, singular-value decomposition (SVD) has been established as an efficient concept to compensate the interferences between the different data streams transmitted over a dispersive channel: SVD is able to transfer the whole system into independent, non-interfering layers exhibiting unequal gains per layer as highlighted in Fig. 9.

The singular-value decomposition (SVD) (Haykin, 2002) of the system matrix **H** results in: $\mathbf{H} = \mathbf{S} \cdot \mathbf{V} \cdot \mathbf{D}^{\mathrm{H}}$, where **S** and $\mathbf{D}^{\mathrm{H}}$ are unitary matrices and **V** is a real-valued diagonal matrix of the positive square roots of the eigenvalues of the matrix $\mathbf{H}^{\mathrm{H}}\mathbf{H}$ sorted in descending order[1].

[1]The transpose and conjugate transpose (Hermitian) of **D** are denoted by $\mathbf{D}^{\mathrm{T}}$ and $\mathbf{D}^{\mathrm{H}}$, respectively.

The MIMO data vector **c** is now multiplied by the matrix **D** before transmission. In turn, the receiver multiplies the received vector **u** by the matrix $\mathbf{S}^{\mathrm{H}}$. In doing so, neither the transmit power budget nor the noise power characteristic is changed. The overall transmission relationship is defined as

$$\mathbf{y} = \mathbf{S}^{\mathrm{H}} (\mathbf{H} \cdot \mathbf{D} \cdot \mathbf{c} + \mathbf{w}) = \mathbf{V} \cdot \mathbf{c} + \tilde{\mathbf{w}}. \tag{8}$$

The unequal gains per layer, i. e., the diagonal element $\sqrt{\xi_{1k}}$ and $\sqrt{\xi_{2k}}$ of the matrix **V** at the time instant *k*, are defined by the positive square roots of the eigenvalues of the matrix $\mathbf{H}^{\mathrm{H}}\mathbf{H}$ (Fig. 9).

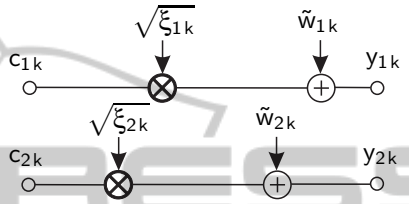

Figure 9: SVD-based layer-specific transmission model.

3 OPTIMIZATION APPROACH

By taking the different layer-specific weighting, introduced by the positive square roots of the eigenvalues of the matrix $\mathbf{H}^{\mathrm{H}}\mathbf{H}$, into account (Fig. 9), bit- and power loading per layer can be used to balance the bit-error probabilities and thus optimize the performance of the whole transmission system. Given a fixed transmission bit rate, the optimization target is a minimum BER: Therefore the bit loading to the different transmission modes is optimized according to the options shown in Table 1.

Table 1: Parameters for bitloading: investigated QAM transmission modes for fixed transmission bit rate.

throughput	layer 1	layer 2
4 bit/s/Hz	16	0
4 bit/s/Hz	4	4
2 bit/s/Hz	4	0
2 bit/s/Hz	2	2

4 CHANNEL-ENCODED MIMO SYSTEM

BICM is constituted by the concatenation of an encoder, an interleaver and a mapper, which is extended here to a BICM-MIMO scheme, where different signal constellations are mapped appropriately to different layers.

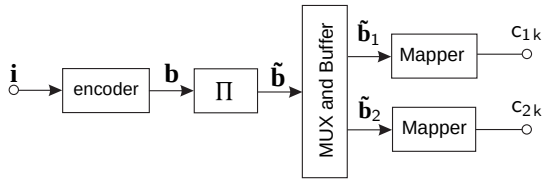

Figure 10: The channel-encoded MIMO transmitter structure.

The channel-encoded transmitter structure is depicted in Fig. 10. The encoder employs a half-rate non-systematic, non-recursive convolutional (NSNRC) code using the generator polynomials $(7,5)$ in octal notation. The uncoded information is organized in blocks of N_i bits, consisting of at least 3000 bits, depending on the specific QAM constellation used. Each data block $\mathbf{i}$ is encoded and results in the block $\mathbf{b}$ consisting of $N_\mathrm{b} = 2N_\mathrm{i} + 4$ encoded bits, including 2 termination bits. The encoded bits are interleaved using a random interleaver and stored in the vector $\tilde{\mathbf{b}}$. The encoded and interleaved bits are then mapped to the MIMO layers. The task of the multiplexer and buffer block of Fig. 10 is to divide the vector of encoded and interleaved information bits, i. e. $\tilde{\mathbf{b}}$, into subvectors according to the chosen transmission mode (Table 1). The individual binary data vectors are then mapped to the QAM symbols c_{1k} and c_{2k} according to the specific mapper used (Fig. 9 and Fig. 10).

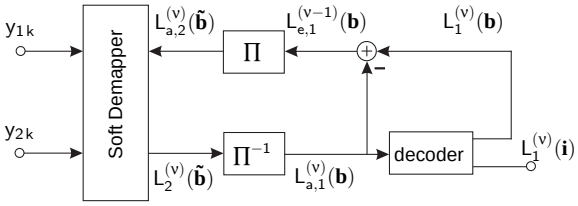

Figure 11: Iterative demodulator structure.

The iterative demodulator structure is shown in Fig. 11 (Ahrens et al., 2008).

When using the iteration index ν, the first iteration of $\nu = 1$ commences with the soft-demapper delivering the N_b log-likelihood ratios (LLRs) $L_2^{(\nu=1)}(\tilde{\mathbf{b}})$ of the encoded and interleaved information bits, whose de-interleaved version $L_{\mathrm{a},1}^{(\nu=1)}(\mathbf{b})$ represents the input of the convolutional decoder as depicted in Fig. 11 (Bahl et al., 1974; Kühn, 2006). This channel decoder provides the estimates $L_1^{(\nu=1)}(\mathbf{i})$ of the original uncoded information bits as well as the LLRs of the N_b NSNRC-encoded bits in the form of

$$L_1^{(\nu=1)}(\mathbf{b}) = L_{\mathrm{a},1}^{(\nu=1)}(\mathbf{b}) + L_{\mathrm{e},1}^{(\nu=1)}(\mathbf{b}) \quad . \tag{9}$$

As seen in Fig. 11 and (9), the LLRs of the NSNRC-encoded bits consist of the receiver's input signal itself plus the extrinsic information $L_{\mathrm{e},1}^{(\nu=1)}(\mathbf{b})$, which is generated by subtracting $L_{\mathrm{a},1}^{(\nu=1)}(\mathbf{b})$ from $L_1^{(\nu=1)}(\mathbf{b})$. The appropriately ordered, i. e. interleaved extrinsic LLRs are fed back as *a priori* information $L_{\mathrm{a},2}^{(\nu=2)}(\tilde{\mathbf{b}})$ to the soft demapper of Fig. 11 for the second iteration.

Following the detailed structure of the soft-demapper in Fig. 12, the N_b LLRs $L_2^{(\nu)}(\tilde{\mathbf{b}})$ are composed of sub-blocks $(L_2^{(\nu)}(\tilde{\mathbf{b}}_1), L_2^{(\nu)}(\tilde{\mathbf{b}}_2))$. Each vector $L_2^{(\nu)}(\tilde{\mathbf{b}}_\ell)$ (with $\ell = 1,2$) is generated by the soft demapper from the MIMO channels' output $y_{\ell,k}$ and the *a priori* information $L_{\mathrm{a},2}^{(\nu)}(\tilde{\mathbf{b}}_\ell)$ (with $\ell = 1,2$) provided by the channel decoder. After the first iteration, this *a priori* information emerges from the N_b LLRs $L_{\mathrm{a},2}^{(\nu)}(\tilde{\mathbf{b}})$.

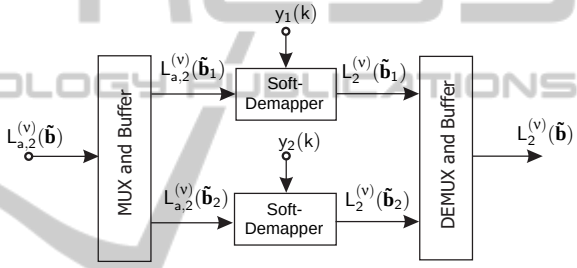

Figure 12: Detailed soft demapper demodulator structure.

5 RESULTS

The numerical analysis targets at BER results. For this purpose it is assumed, that each optical input within the multimode fiber is fed by a system with identical mean properties with respect to transmit filter and pulse frequency $f_\mathrm{T} = 1/T_\mathrm{s}$. For numerical assessment within this paper, the pulse frequency is chosen to be $f_\mathrm{T} = 5{,}12$ GHz, the average transmit power is supposed to be $P_\mathrm{s} = 1\,\mathrm{V}^2$ – this equals 1 W at a linear and constant resistance of $1\,\Omega$ – and as an external disturbance a white Gaussian noise with power spectral density N_0 is assumed (Pankow et al., 2011). In order to transmit at a fixed data rate while maintaining the best possible integrity, i. e., bit-error rate, an appropriate number of MIMO layers has to be used, which depends on the specific transmission mode, as detailed in Tab. 1.

5.1 Uncoded MIMO System

The optimization results, obtained by computer simulation at an overall data rate of 20,48 Gbps, are shown

in Fig. 13 for different operating wavelength: The BER becomes minimal in case of an optimized bit loading (Fig. 13) with highest bit loading in the layer with largest singular values. The optimized MIMO transmission exhibits an improvement with respect to SISO transmission, but a non-optimized MIMO transmission leads to a significant degradation of the system performance. Furthermore, the simulation results show that in order to minimize the overall BER at a fixed data rate, not necessarily all MIMO layer should be activated. Instead, only the strongest MIMO layers should be used with appropriate modulation levels in the considered example.

Furthermore, as obtained by the channel measurements (Fig. 3 and Fig. 4), at a higher operating wavelength, i. e. 1570 nm, the separation of the different mode groups disappears based on the effect of the chromatic dispersion. Since the chromatic dispersion affects all mode groups almost equally, MIMO isn't able to generate an additional diversity gain (in comparison to wireless channels, where delay-spread isn't any longer a limiting parameter (Ahrens and Benavente-Peces, 2009b; Ahrens and Benavente-Peces, 2011)). The advantage of a higher signal-to-noise-ratio due to lower attenuation in the third optical window is diminished by the chromatic dispersion. Therefore, the obtained bit-error rate results are higher at 1570 nm compared to 1325 nm. However, dispersion compensation schemes are well established in optical communications and they are not considered as a practical limitation.

However, uncoded systems have reached a state of maturity. By contrast coded MIMO configurations require substantial further research.

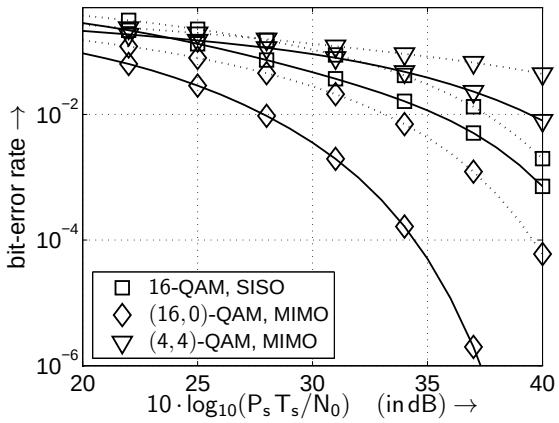

Figure 13: BER performance at 1570 nm operating wavelength (dotted line) and at 1325 nm operating wavelength (solid line) when using the transmission modes introduced in Tab. 1 and transmitting 4 bit/s/Hz over frequency selective optical MIMO channels.

5.2 Channel Encoded MIMO System

The joint optimization of the number of activated MIMO layers as well as the number of bits per symbol was found to be effective at high SNRs. However, iterative receivers are able to work in a much lower SNR region. Therefore it would be interesting to see how the design criteria change when coding is added to the transmission system.

Using the half-rate, constraint-length $K_{\mathrm{cl}} = 3$ NSNRC code with the generator polynomials of $(7,5)$ in octal notation, the BER performance is analyzed for an effective throughput of 2 bit/s/Hz based on the best uncoded schemes of Table 1. In addition to the number of bits per symbol and the number of activated MIMO layers, the achievable performance of the iterative decoder is substantially affected by the specific mapping of the bits to both the QAM symbols as well as to the MIMO layers. Here, the maximum iteration gain can only be guaranteed, if anti-Gray mapping is used on all activated MIMO layers (Chindapol, 2001).

Furthermore, observed by comparing the extrinsic information transfer (EXIT) chart results of Fig. 14 and 15, the overall performance is strongly influenced by the allocation of the number of bits to the MIMO layers.

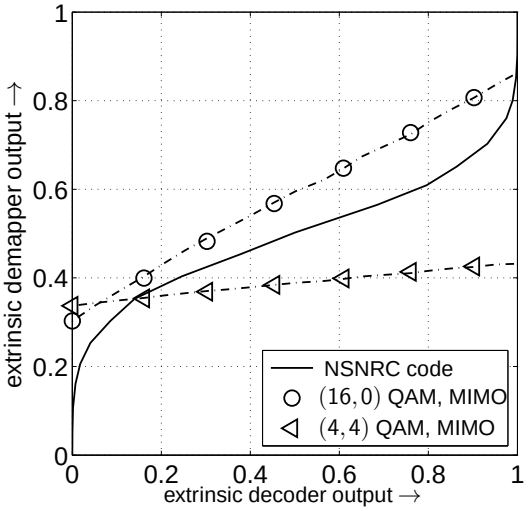

Figure 14: EXIT chart for an effective user-data throughput of 2 bit/s/Hz and the different QAM constellations at $10\log_{10}(P_s T_s/N_0) = 18$ dB (1325 nm operating wavelength and anti-Gray mapping on all activated MIMO layers).

In order to guarantee an open EXIT tunnel and therefore an efficient information exchange between the soft demapper transfer characteristic and the decoder transfer characteristic at a given signal-to-noise

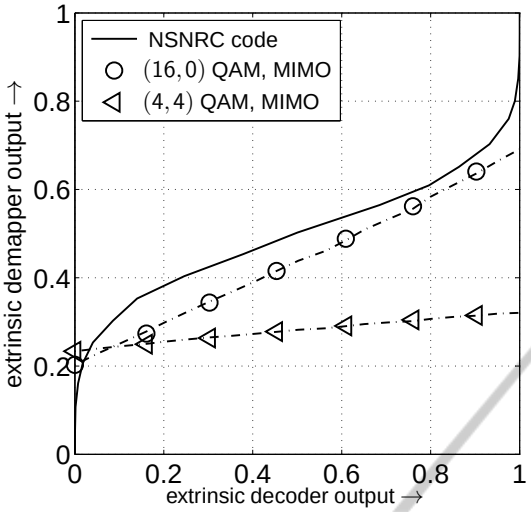

Figure 15: EXIT chart for an effective user-data throughput of 2 bit/s/Hz and the different QAM constellations at $10\log_{10}(P_s T_s/N_0) = 18$ dB (1570 nm operating wavelength and anti-Gray mapping on all activated MIMO layers).

ratio, not necessarily all MIMO should be activated. In the considered example only the strongest MIMO layer should be used with appropriate modulation level. Activating all MIMO layers the information exchange between the soft demapper and the decoder stops relatively early, resulting in a reduced BER performance.

Furthermore, it turns out that chromatic dispersion combined with the specific QAM constellation sizes, as detailed in Tab. 1, leads to a degradation of the overall performance as expected.

The BER performance is presented in Fig. 16 based on the different schemes of Table 1 and confirms the EXIT chart results. The information word length is 3000 bits and a random interleaver is applied.

Fig. 17 illustrates the wavelength-dependent BER performance. As already stated by the EXIT charts results, the chromatic dispersion leads to a degradation of the overall performance.

The inferior performance is also indicated by the corresponding BER curves shown in Fig. 17.

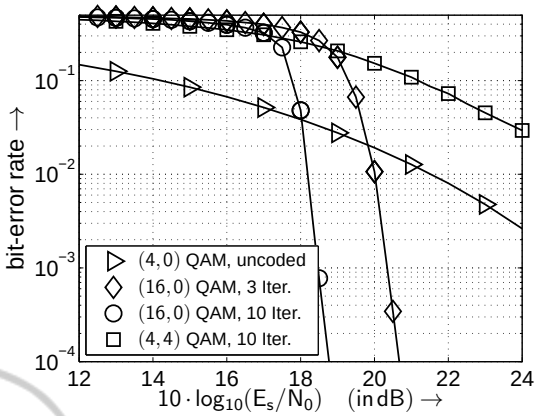

Figure 16: BERs assuming anti-Gray mapping scheme on the activated MIMO layers for an effective user-data throughput of 2 bit/s/Hz (1325 nm operating wavelength).

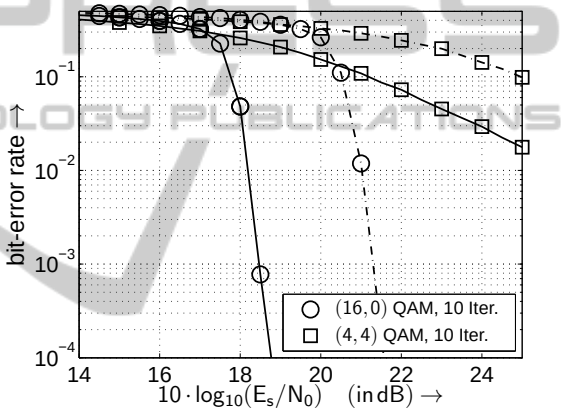

Figure 17: BER comparison at 1325 nm operating wavelength (solid line) and at 1570 nm operating wavelength (dotted line) assuming anti-Gray mapping scheme on the activated MIMO layers for an effective user-data throughput of 2 bit/s/Hz.

6 CONCLUSIONS

Coherent MIMO transmission over measured multimode optical fibers has been investigated targeting at minimized BER while keeping the transmission bitrate constant. The results show that MIMO transmission based on SVD is a promising approach, in particular when the bit loading is optimized. In that case significant BER improvements can be achieved compared to a conventional SISO system. The proposed MIMO-BICM scheme includes an adaptation of the transmit parameters. EXIT charts are used for analysing and optimizing the convergence behaviour of iterative demapping and decoding. Here, the choice of the number of bits per symbol and the number of MIMO layers combined with powerful error correcting codes substantially affects the performance of a MIMO system, suggesting that not all MIMO layers have to be activated in order to achieve the best BERs.

ACKNOWLEDGEMENTS

The authors wish to thank their co-worker, Mr. Steffen Schröder, for supporting the measurement cam-

paign.

REFERENCES

Ahrens, A. and Benavente-Peces, C. (2009a). Modulation-Mode and Power Assignment for Broadband MIMO-BICM Schemes. In *IEEE 20th Personal, Indoor and Mobile Radio Communications Symposium (PIMRC)*, Tokio (Japan).

Ahrens, A. and Benavente-Peces, C. (2009b). Modulation-Mode and Power Assignment in Broadband MIMO Systems. *Facta Universitatis (Series Electronics and Energetics)*, 22(3):313–327.

Ahrens, A. and Benavente-Peces, C. (2011). Modulation-Mode Assignment in Iteratively Detected and SVD-assisted Broadband MIMO Systems. In Filipe, J. and Obaidat, M. S., editors, *E-business and Telecommunications*, Communications in Computer and Information Science, pages 307–319. Springer, Berlin, Heidelberg.

Ahrens, A. and Lange, C. (2006). Exploitation of Far-End Crosstalk in MIMO-OFDM Twisted Pair Transmission Systems. In *IASTED International Conference on Wireless Networks and Emerging Technologies (WNET)*, Banff, Alberta (Kanada).

Ahrens, A., Ng, S. X., Kühn, V., and Hanzo, L. (2008). Modulation-Mode Assignment for SVD-Aided and BICM-Assisted Spatial Division Multiplexing. *Physical Communications (PHYCOM)*, 1(1):60–66.

Bahl, L. R., Cocke, J., Jelinek, F., and Raviv, J. (1974). Optimal Decoding of Linear Codes for Minimizing Symbol Error Rate. *IEEE Transactions on Information Theory*, 20(3):284–287.

Baliga, J., Ayre, R., Hinton, K., Sorin, W. V., and Tucker, R. S. (2009). Energy Consumption in Optical IP Networks. *Journal of Lightwave Technology*, 27(13):2391–2403.

Bülow, H., Al-Hashimi, H., and Schmauss, B. (2010). Stable Coherent MIMO Transport over Few Mode Fiber Enabled by an Adiabatic Mode Splitter. In *European Conference and Exhibition on Optical Communication (ECOC)*, page P4.04, Torino, Italy.

Bülow, H., Al-Hashimi, H., and Schmauss, B. (2011). Coherent Multimode-Fiber MIMO Transmission with Spatial Constellation Modulation. In *European Conference and Exhibition on Optical Communication (ECOC)*, Geneva, Switzerland.

Caire, G., Taricco, G., and Biglieri, E. (1998). Bit-Interleaved Coded Modulation. *IEEE Transactions on Information Theory*, 44(3):927–946.

Chindapol, A. Ritcey, J. A. (2001). Design, Analysis, and Performance Evaluation for BICM-ID with square QAM Constellations in Rayleigh Fading Channels. *IEEE Journal on Selected Areas in Communications*, 19(5):944–957.

Foschini, G. J. (1996). Layered Space-Time Architecture for Wireless Communication in a Fading Environment when using Multiple Antennas. *Bell Labs Technical Journal*, 1(2):41–59.

Haykin, S. S. (2002). *Adaptive Filter Theory.* Prentice Hall, New Jersey.

Hsu, R. C. J., Tarighat, A., Shah, A., Sayed, A. H., and Jalali, B. (2006). Capacity Enhancement in Coherent Optical MIMO (COMIMO) Multimode Fiber Links. *IEEE Communications Letters*, 10(3):195–197.

Kühn, V. (2006). *Wireless Communications over MIMO Channels – Applications to CDMA and Multiple Antenna Systems.* Wiley, Chichester.

Lenz, D., Rankov, B., Erni, D., Bächtold, W., and Wittneben, A. (2004). MIMO Channel for Modal Multiplexing in Highly Overmoded Optical Waveguides. In *International Zurich Seminar on Communications (IZS)*, Zurich,Switzerland.

Pankow, J., Aust, S., Lochmann, S., and Ahrens, A. (2011). Modulation-Mode Assignment in SVD-assisted Optical MIMO Multimode Fiber Links. In *15th International Conference on Optical Network Design and Modeling (ONDM)*, Bologna (Italy).

Pickavet, M., Vereecken, W., Demeyer, S., Audenaert, P., Vermeulen, B., Develder, C., Colle, D. Dhoedt, B., and Demeester, P. (2008). Worldwide Energy Needs for ICT: the Rise of Power-Aware Networking. In *International Symposium on Advanced Networks and Telecommunication Systems (ANTS)*, Bombay, India.

Raleigh, G. G. and Cioffi, J. M. (1998). Spatio-Temporal Coding for Wireless Communication. *IEEE Transactions on Communications*, 46(3):357–366.

Shah, A., Hsu, R. C. J., Tarighat, A., Sayed, A. H., and Jalali, B. (2005). Coherent Optical MIMO (COMIMO). *Journal Of Lightwave Technology*, 23(8):2410–2419.

Singer, A. C., Shanbhag, N. R., and Bae, H.-M. (2008). Electronic Dispersion Compensation – An Overwiew of Optical Communications Systems. *IEEE Signal Processing Magazine*, 25(6):110 – 130.

Telatar, E. (1999). Capacity of Multi-Antenna Gaussian Channels. *European Transactions on Telecommunications*, 10(6):585–595.

Van Etten, W. (1975). An Optimum Linear Receiver for Multiple Channel Digital Transmission Systems. *IEEE Transactions on Communications*, 23(8):828–834.